Trap-induced shape resonances in an ultracold few-body system of an atom and static impurities

Marta Sroczyńska,[1] Tomasz Wasak,[1] Krzysztof Jachymski,[1,2] Tommaso Calarco,[3] and Zbigniew Idziaszek[1]
[1]*Faculty of Physics, University of Warsaw, ul. Pasteura 5, PL-02-093 Warsaw, Poland*
[2]*Institute for Theoretical Physics III & Center for Integrated Quantum Science and Technology (IQST), University of Stuttgart, Pfaffenwaldring 57, D-70550 Stuttgart, Germany*
[3]*Institute for Complex Quantum Systems & Center for Integrated Quantum Science and Technology (IQST), Universität Ulm, Albert-Einstein-Allee 11, D-89075 Ulm, Germany*

(Received 15 February 2018; revised manuscript received 5 June 2018; published 16 July 2018)

Hybrid systems of ultracold atoms and trapped ions or Rydberg atoms can be useful for quantum simulation purposes. By tuning the geometric arrangement of the impurities, it is possible to mimic solid-state and molecular systems. Here, we study a single trapped atom interacting with a set of arbitrarily arranged static impurities and show that the problem admits an analytical solution. We analyze in detail the case of two impurities, finding multiple trap-induced resonances which can be used for entanglement generation. Our results serve as a building block for the studies of quantum dynamics of complex systems.

DOI: 10.1103/PhysRevA.98.012708

I. INTRODUCTION

Ultracold trapped atoms have found numerous applications in the field of quantum simulations of many-body physics [1]. Properties of ultracold atomic systems can be tuned in experiment using external electromagnetic fields, which provide the opportunity to shape the trapping potential experienced by the atoms [2] as well as their interactions [3]. Both bosonic and fermionic atomic species are available. These favorable properties lead to a number of accomplishments with ultracold atoms in optical lattices such as observation of superfluid-Mott insulator transition [4], superexchange interactions for simulations of spin lattice Hamiltonians [5], many-body localized phases of matter [6], or exotic quantum states such as the supersolid phase [7,8]. Quantum computation schemes involving cold atoms have also been proposed based on various mechanisms such as state-dependent potentials, exchange interactions, trap-induced resonances, and other [9–15].

In recent years, great progress has been made in realization of other quantum technology platforms such as trapped ions and Rydberg atoms [16–19]. Interestingly, trapped ions and cold atoms can be combined into a novel hybrid quantum system [20]. Such systems allow for study of multiatom single-ion molecular processes [21]. A chain of trapped ions can act as a periodic external potential for cold atoms, emulating a solid state with atoms playing the role of mobile electrons [22]. Another promising hybrid system involves trapped Rydberg atoms acting as impurities instead of ions. Rydberg atoms can be arranged in arbitrary three-dimensional structures using optical tweezers [23–26]. In a similar way to the solid-state simulation [22], one can view hybrid systems as potential simulators of complex molecular phenomena such as formation and reconfiguration of chemical bonds or excitation transport in macromolecules. Here, the atoms would play the role of electrons and the impurities would mimic nuclear cores.

To further increase the potential of such systems and uncover their novel applications, the interaction of a single atom with other particles needs to be understood first. This is similar to finding natural orbitals of a molecular system. In this work, we make a first step in this direction by showing that the problem of finding the eigenstates of a single harmonically trapped atom interacting with arbitrarily many impurities can be approached analytically in the limit of the low collision energy, when the atom-ion interaction can be modeled with the s-wave regularized delta pseudopotential [27]. We provide a general method of solving the Schrödinger equation describing such a system based on free function method [28], along with its application to a simple case of two impurities.

The structure of this paper is organized as follows. In Sec. II, we first introduce the general Hamiltonian of a trapped atom interacting with many static impurities. Then, we present the method based on Green's function formalism that reduces the problem of solving the Schrödinger equation to a search of the roots of a single function expressed in terms of the Green's functions. The details of the derivation are described in Appendix A. In Sec. III, we apply this general method to a system consisting of a single harmonically trapped atom interacting with two static impurities. For the case of symmetrically placed impurities, we calculate the lowest-energy levels as a function of the distance between the impurities and the atom-impurity scattering length. In addition, we compare the obtained results with a variational approach exploiting a simple trial wave function. We provide also the analysis of the avoided crossings that appear in such a system due to the trap-induced resonances. A summary of the results and the feasibility of the molecular simulator are provided in Sec. IV.

II. MODEL

In this section, we first describe the Hamiltonian of the system, and then present the method of solving the stationary states of the system. The procedure we follow is based on the Green's function approach, and the method yields the energies and wave functions of the particle interacting with

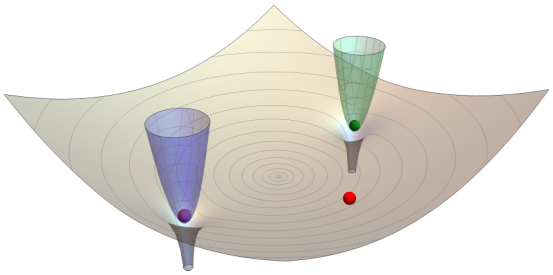

FIG. 1. An interaction potential experienced by a trapped atom (red sphere) in the presence of two localized impurities (purple and green spheres), which are localized by external trapping potentials (purple and green). In the vicinity of the static particles, the trapping potential is modified by the atom-impurity interaction; the gray surface is the effective potential experienced by the atom.

the impurities. Since the interaction between the particles is effectively zero ranged, the whole description of the problem is reduced to finding zeros of a simple function, given by a determinant of a finite, known matrix.

The few-body system studied in this work is composed of a single atom and many impurities. We assume that each impurity is trapped tightly by its separate external trapping potential. We consider the impurities to be localized at predetermined positions and refer to them as static impurities. An example of such a situation is displayed in Fig. 1, where a single atom moves in a harmonic trapping potential with two different impurities localized by separate traps (purple and green potentials in the figure). The atom-impurity interaction is assumed to be local, i.e., the characteristic interaction range is much smaller than other length scales such as the trap size and de Broglie wavelength.

The Hamiltonian of a trapped atom interacting with N static impurities is given by

$$H = -\frac{\hbar^2}{2m}\Delta + V_{\mathrm{tr}}(\mathbf{r}) + \sum_{i=1}^{N} V_{\mathrm{ai}}(\mathbf{r}_i), \tag{1}$$

where V_{tr} denotes the trapping potential, and $\mathbf{r}_i = \mathbf{r} - \mathbf{d}_i$ is the position of the atom with respect to the ith impurity. We approximate the true atom-impurity interaction potential by the contact pseudopotential

$$V_{\mathrm{ai}}(\mathbf{r}_i) = g_i \delta(\mathbf{r}_i)\frac{\partial}{\partial r_i} r_i. \tag{2}$$

Here, the parameter $g_i = 2\pi\hbar^2 a_i/m$ is the coupling strength, which is expressed in terms of the effective atom-impurity scattering length a_i and the mass m of the atom. Note that we allow the atom to interact with each impurity with its own potential, so the coupling strength g_i can depend on the index i of the impurity. The contact potential approximation is valid [10,29,30] provided that the characteristic scales of length and energy, denoted, respectively, by R^* and E^*, of the interaction potential fulfill the following conditions: $l_0 \gg R^*$, $d_{i,j} \gg R^*$, and $E^* \gg E_0$, where l_0 is the characteristic length of the trapping potential, $d_{i,j} = |\mathbf{d}_i - \mathbf{d}_j|$ is the distance between the impurities, and E_0 denotes the characteristic energy scale of the trap (see Fig. 2). As the typical length scales on which the traps can be operated are of the order of micrometers and

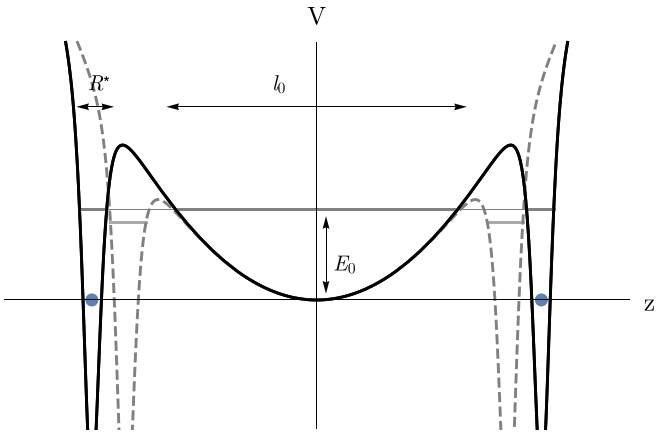

FIG. 2. The mechanism of the resonance and the characteristic length and energy scales in the system. If the bound states of the atom-impurity potential are at the same level as the bound state in the trap (solid line potential), there is a resonance and the avoided crossing appears (see, e.g., Fig. 3 or 8). The wave function for such state is a mixture of the trap state and the states localized on the impurities [see Figs. 7(d), 7(f), and the text for details]. Dashed line potential depicts a situation when the bound states of the atom-impurity potential are at different positions (dashed line potential) than the bound state of the trap, and the system is far from the avoided crossing.

the value of $R^\star$ can range from ∼100 Bohr radii a_0 for neutral atoms to ∼5000 for ion-atom systems, this separation is usually fulfilled.

The Hamiltonian from Eq. (1) leads to the following time-independent Schrödinger equation:

$$\left[-\frac{\hbar^2}{2m}\Delta + V(\mathbf{r}) + \sum_{i=1}^{N} g_i \delta(\mathbf{r}_i)\frac{\partial}{\partial r_i} r_i\right]\Psi(\mathbf{r}) = E\Psi(\mathbf{r}). \tag{3}$$

In order to find the eigenstates of this equation, we start by expanding the (yet unknown) wave function $\Psi(\mathbf{r})$ in the basis states $\phi_{\mathbf{n}}(\mathbf{r})$, so that $\Psi(\mathbf{r}) = \sum_{\mathbf{n}} c_{\mathbf{n}}\phi_{\mathbf{n}}(\mathbf{r})$. We use the basis in which the noninteracting part of the Hamiltonian is diagonal. To find the wave function Ψ, we insert its expansion in the chosen basis into Eq. (3) and obtain a set of equations for the coefficients $c_{\mathbf{n}}$ (see Appendix A for details of the derivation). The result yields

$$\Psi(\mathbf{r}) = \sum_{i=1}^{N}\sum_{\mathbf{n}} g_i k_i \frac{\phi^*_{\mathbf{n}}(\mathbf{d}_i)\phi_{\mathbf{n}}(\mathbf{r})}{E - E_{\mathbf{n}}}, \tag{4}$$

where k_i are given by

$$k_i = \left[\frac{\partial}{\partial r_i} r_i \Psi(\mathbf{r})\right]\Big|_{\mathbf{r}=\mathbf{d}_i}. \tag{5}$$

The solution Ψ depends on the coefficients k_i, which in turn depend on Ψ. Therefore, solution has to be found in a self-consistent way.

To proceed with the construction of Ψ and evaluation of k_i, we first recall the expression for the Green's function (see Appendix B fore more details):

$$G(\mathbf{d}_i, \mathbf{r}) = \sum_{\mathbf{n}} \frac{\phi^*_{\mathbf{n}}(\mathbf{d}_i)\phi_{\mathbf{n}}(\mathbf{r})}{E - E_{\mathbf{n}}}. \tag{6}$$

Note that G depends on the energy E, but we dropped this dependence in the notation for brevity. We then insert the solution for Ψ from Eq. (4) into Eq. (5), and rewrite it using Eq. (6) to finally arrive at

$$k_i = \sum_{j=1}^{N} g_j k_j \left[\frac{\partial}{\partial r_i} r_i G(\mathbf{d}_j,\mathbf{r})\right]\Big|_{\mathbf{r}=\mathbf{d}_i}. \tag{7}$$

This is a linear equation for the coefficients k_i, and it can be put into the matrix form

$$\hat{D}_N \cdot \vec{k} = 0, \tag{8}$$

where $\vec{k} = (k_1,\ldots,k_N)$ and the matrix

$$\hat{D}_N(E) = \begin{pmatrix} g_1 G_{\mathrm{r}}(\mathbf{d}_1,\mathbf{d}_1)-1 & \ldots & g_N G(\mathbf{d}_N,\mathbf{d}_1) \\ \vdots & \ddots & \vdots \\ g_1 G(\mathbf{d}_1,\mathbf{d}_N) & \ldots & g_N G_{\mathrm{r}}(\mathbf{d}_N,\mathbf{d}_N)-1 \end{pmatrix}, \tag{9}$$

where the regularized Green's function, which appears on the diagonal of $\hat{D}_N$, is $G_{\mathrm{r}}(\mathbf{d}_i,\mathbf{d}_i) = [\frac{\partial}{\partial r_i} r_i G_E(\mathbf{d}_i,\mathbf{r})]|_{\mathbf{r}=\mathbf{d}_i}$. Note that the matrix $\hat{D}_N$ depends on the energy E only through the Green's function. The Green's function for the trapping potential can be given either analytically or it can be calculated numerically [31,32]. The diagonal elements of $\hat{D}_N(E)$ can be then calculated assuming the following expansion of the Green's function:

$$G(\mathbf{r},\mathbf{r}') \xrightarrow[|\Delta\mathbf{r}|\to 0]{} g^0(\mathbf{R}) + \frac{g^1(\mathbf{R})}{|\Delta\mathbf{r}|}, \tag{10}$$

where $\Delta\mathbf{r} = \mathbf{r} - \mathbf{r}'$ and $\mathbf{R} = (\mathbf{r}+\mathbf{r}')/2$. The regularization then leads to $\hat{D}_N^{ii}(E) = g^0(\mathbf{d}_i)$. In Appendix B, we provide the expressions for $g^0(R)$ and $g^1(R)$ for the spherically symmetric harmonic potential [see Eq. (B11a)]. In such a case, the functions g^0 and g^1 depend only on radius $R = |\mathbf{R}|$.

Solutions of Eq. (8) exist provided that the determinant of $\hat{D}_N$ is equal to 0. For fixed positions $\mathbf{d}_i$ and coupling strengths g_i, the determinant is a function of a single variable E only, and its roots are identified as the eigenenergies of the system, i.e., $\det\hat{D}_N(E_n) = 0$ for the nth stationary state. For each eigenenergy E_n, the corresponding wave function, expressed in terms of k_i [see Eq. (4)] is obtained by evaluating the kernel (the null space) of the matrix $\hat{D}_N(E_n)$.

III. TWO IMPURITIES IN A HARMONIC TRAP

With the general solution at hand, we now consider a single atom interacting with two impurities that are located at positions $\mathbf{d}_1$ and $\mathbf{d}_2$ in a spherical harmonic trap with frequency ω. We assume that all the scattering lengths are the same and equal to a. To simplify the notation, we transform the problem into dimensionless units of oscillator length and energy, $l_0 = \sqrt{\hbar/m\omega}$ and $E_0 = \hbar\omega$, respectively. The dimensionless coupling strength, naturally entering into the problem in the place of the coupling $g_i = g$, is then equal to $\gamma = 2\pi a/l_0$.

The stationary states, their energies, and wave functions are calculated from Eq. (8). Here, $\vec{k} = (k_1,k_2)$, and the matrix $\tilde{D}(E) \equiv \hat{D}_2(E)/\gamma$ stems from Eq. (9):

$$\tilde{D}(E) = \begin{pmatrix} G_{\mathrm{r}}(\mathbf{d}_1,\mathbf{d}_1) - \gamma^{-1} & G(\mathbf{d}_2,\mathbf{d}_1) \\ G(\mathbf{d}_1,\mathbf{d}_2) & G_{\mathrm{r}}(\mathbf{d}_2,\mathbf{d}_2) - \gamma^{-1} \end{pmatrix}. \tag{11}$$

Since in the matrix $\tilde{D}(E)$ the rows and columns are linearly dependent, only the ratio of k_i can be evaluated, i.e., $k_1/k_2 = -[\tilde{D}(E)]_{12}/[\tilde{D}(E)]_{11}$. The absolute values of k_i can then be determined from the normalization condition for Ψ in Eq. (4). The required Green's function in this case can be evaluated analytically; the necessary formulas are given in Appendix B. Note that the regularized Green's function, necessary for the diagonal elements of the matrix in Eq. (11), is equivalent to the function $g^0(\mathbf{d}_i)$, given by Eq. (B11a), in the expansion (10) of the full Green's function.

A. Symmetric case

Below we focus on the case of two impurities placed symmetrically with respect to the origin $\mathbf{d}_1 = -\mathbf{d}_2 = \mathbf{d}$. We assume that the impurities are located on the z axis, and we take $\mathbf{d} = (0,0,d)$. Note that the distance between the impurities is equal to $2d$.

To find the energies, we search for the roots of $\det\tilde{D}(E)$ given by Eq. (11). First, we calculate the energies of the system for different values of the distance $2d$ between the impurities and different scattering length a characterizing the atom-impurity interaction.

Figure 3 presents the dependence of the energy levels of the system on the impurities' positions for six different values of $a/l_0 = \pm 0.4$, ± 1.0, and ± 10. In general, the eigenstates can be classified according to the symmetry $z \to -z$ of the Hamiltonian into even and odd states, denoted in the figure with blue dotted and red dashed lines, respectively. As can be observed from the figure, for very large separations between the impurity atoms, the energy spectrum approaches the spectrum of the unperturbed harmonic oscillator $E_n^{\mathrm{ho}} = \hbar\omega(n+3/2)$ with $n = 0,2,4,\ldots$ for even and $n = 1,3,5,\ldots$ for odd states. For separations comparable to the oscillator length, the observed energies deviate from the harmonic oscillator case due to the presence of the impurities. For separations between the impurities much smaller than the other length scales of the model (a and l_0), when the distance d is of the order of the interaction range of the true potential, the description of the interaction in terms of the contact pseudopotential is no longer valid. Interestingly, the odd states do not feel the contact potential for $d = 0$, recovering the unperturbed harmonic oscillator limit in this case, but the even states for $d = 0$ do not approach the results obtained by Busch [33] for a single impurity. In the limit $d \to 0$, our model in terms of two separate regularized delta potentials is no longer valid.

Let us first discuss the results for negative a presented in the bottom row in Fig. 3. In the case of $a = -0.4l_0$ [see Fig. 3(d)], we observe relatively small perturbation compared to the harmonic oscillator case. The energy shift becomes larger with increasing magnitude of the scattering length a [see Figs. 3(e) and 3(f)]. However, for small d, when the harmonic potential is negligible, the energy of the atom is negative, indicating the presence of a bound state.

To identify the lowest energies of the atom with bound states for small d, we calculate the bound-state energies of the atom in free space, with neglected trapping potential. To this end, we refer to Eq. (11), when now G denotes the Green's function of the atom in free space. The results, i.e., the roots of $\det\tilde{D}(E)$ with $E < 0$, are depicted in Fig. 3 with gray solid lines. In free

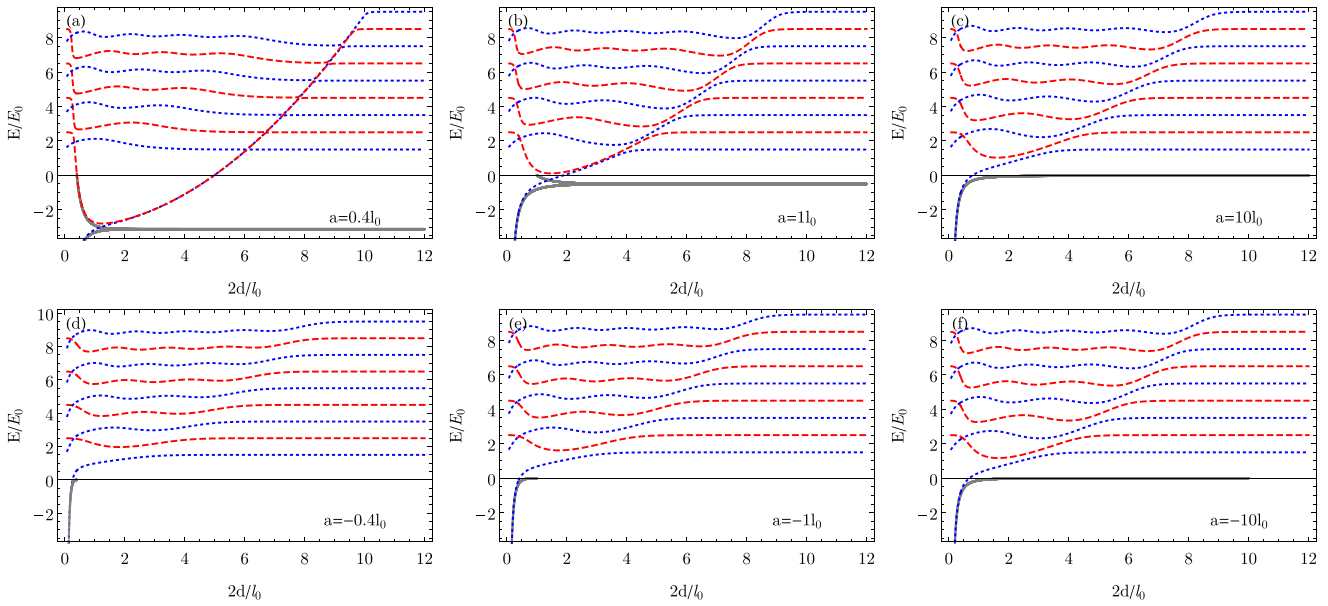

FIG. 3. The lowest-energy levels of the atom as a function of the distance between the impurities, equal to $2d$, for different values of the scattering length a. The dotted blue and dashed red lines denote even and odd states, respectively. The solid gray lines display the energy levels of the bound states ($E < 0$) in absence of the trap.

space, for $a < 0$, only even bound states (with $E < 0$) exist if $2d < |a|$. At $2d = |a|$, the energy of the state crosses the zero threshold and enters into the continuum.

Let us now turn to the positive values of the scattering length a [see Fig. 3(a)]. At large separation between the impurities, the lowest state is a doubly degenerate superposition of dimer bound states. The energy of the dimer in free space approaches $-\hbar^2/2ma^2$, but it is lifted quadratically in our case due to the external harmonic trap. At small separations, the trapping potential is negligible and the splitting between the bound states of different symmetry becomes significant. The state lower in energy is always even and the higher is odd.

We note that the energy of the odd molecular state increases with decreasing separation between impurities. At sufficiently small separations, the odd molecular state cannot exist in free space since it enters the continuum, as can be observed from Fig. 3(a) or 3(b) (gray line). In the presence of the trap, the odd molecular state survives as there is no continuum, but its energy still increases with decreasing separation. As a result, the odd-state energy can turn out to be larger than the first trap-extended even state, and so the first two lowest-energy levels of the system are of even character. This odd molecular state forms avoided crossing with trap-extended odd states, as can be most clearly observed in Fig. 3(a).

For larger scattering lengths, the odd state can even be pushed into the continuum [compare Figs. 3(b) and 3(c)]. We note that the splitting between the bound states decays exponentially with the distance, as is the case for the H_2^+ molecule [34]. The system considered here acts as a precursor for molecular physics simulation by reproducing the core features of the simplest possible molecule.

In general, avoided crossings appear due to the trap-induced shape resonance mechanism [10]. Each of the potentials, describing impurity-atom interaction, can support a bound state. Its energy can be lifted above the zero-energy threshold by the external potential. If the total energy is brought into degeneracy with this bound state, a the trap-induced resonance occurs. This is similar to the simpler case of two harmonically trapped atoms studied in [35], but more complex due to the reflection symmetry present in our problem.

Avoided crossings in the spectrum represent resonances and breakdown of the perturbation theory. Trap-induced shape resonances have been shown to be useful for controlling the quantum state of the system. Below, we recall only a few examples. The avoided crossings due to the trap-induced shape resonances can be applied to perform two-atom quantum logic gates [10], for spectroscopy and coherent control of ultracold molecular dimers, and production of ultracold molecules tunable by the trap parameters. In [35], these resonances were applied for two purposes: construction of a quantum phase gate and coherent transfer of particles into higher Bloch bands in an optical lattice. In [36], the trap-induced shape resonances in reduced dimensionalities were used for quantum state control and spectroscopy of atom-ion molecules. In [13], resonances due to traps were exploited for construction of a fast two-qubit quantum phase gate between an atom and an ion. In [15], trap-induced shape resonances were studied in external double-well trapping potential, and proposed to perform fast quantum gate operation by applying an external magnetic field leading to Feshbach resonances. In our case, trap-induced shape resonances are due to the degeneracy of molecular states between many impurities and trap-extended states. Therefore, our setup allows not only for generation of entangled states or quantum gates operations between two particles, but also for realization of quantum state control, and coherent transfer of population from trap-extended states into superposition of molecular states localized in two separate spatial regions. Such states might prove useful for generation of many-particle entangled states, or for metrological and quantum information

processing applications, and for simulations of molecular systems from quantum chemistry.

In Fig. 3(a), we observe narrow avoided crossings since the scattering length is small, and thus the coupling between the levels is weak. The splitting in the avoided crossings increases with growing a, as can be observed from Figs. 3(b) and 3(c). The reflection symmetry of the system with respect to $z \to -z$ implies the presence of a state of different symmetry between each two states of the same symmetry experiencing an avoided crossing. Specifically, at the positions of the avoided crossings in Figs. 3(a)–3(c), between each two energy levels of the same symmetry (the same color) there is a state of different symmetry (of other color). This effect originates from the presence of two bound states, which are almost degenerate, but have different symmetries and do not couple with each other.

To understand the properties of the avoided crossing between the extended states and the bound states in trap, we turn to a simpler description. We adopt the variational approach in which we make the following ansatz:

$$\Psi(\mathrm{r}) = v_1\psi_1(\mathbf{r}) + v_2\psi_2(\mathbf{r}), \tag{12}$$

where the normalized wave function $\psi_i(\mathbf{r}) = \psi(\mathbf{r} - \mathbf{d}_i)$, and the free-space wave function of the bound state is $\psi(\mathbf{r}) = \exp(-r/a)/(\sqrt{2\pi a r})$. Therefore, the wave function is a linear combination of states that describe an atom localized around each impurity. The minimum of the energy is achieved for v_i that satisfy

$$\begin{pmatrix} H_{11} - E & H_{12} - ES_{12} \\ H_{21} - ES_{21} & H_{22} - E \end{pmatrix} \begin{pmatrix} v_1 \\ v_2 \end{pmatrix} = 0, \tag{13}$$

where the matrix elements of the Hamiltonian are denoted by $H_{ij} = \langle\psi_i|H|\psi_j\rangle$, and the overlap between the states is $S_{ij} = \langle\psi_i|\psi_j\rangle$. We solve the resulting equations numerically.

The results of the variational approach are presented in Fig. 4. The bound states of different symmetries (for odd states we have $v_1 = -v_2$ whereas for even $v_1 = v_2$) are displayed for positive scattering lengths $a = 0.4\,l_0$ and l_0 in Figs. 4(a) and 4(b), respectively. Even though the approximate wave function works well reproducing the overall trend, the approach is missing the quantitative description of the avoided crossings. Furthermore, the approximation breaks down when the distance between the impurities is comparable to the scattering length, and the overlap S_{12} deviates significantly from zero. In all the other cases, i.e., for larger impurity separations and away from the avoided crossing, the variational calculation is accurate.

To improve the approximate description of the wave function in variational approach, we include into Eq. (12) a third state, which corresponds to an extended state (occupying the whole volume of the trap) of the unperturbed harmonic oscillator. For illustration, we will only consider the lowest trap-induced shape resonance, which occurs for $a/l_0 = 0.4$ at $2d/l_0 \approx 6$. To this end, we add a third state $\psi_3(\mathbf{r}) = \phi_0(\mathbf{r})$, where $\phi_0(\mathbf{r}) \propto \exp(-r^2/2l_0^2)$ is the normalized ground-state wave function of the harmonic oscillator, with its corresponding amplitude v_3 on the right-hand side in Eq. (12). The minimization of the mean energy with such an ansatz yields the energy as a function of the distance $2d$ between the impurities. Note that the same results are obtained in a two-state model with appropriate symmetry of the participating states, i.e., an even trap-extended state and an even superposition of localized states.

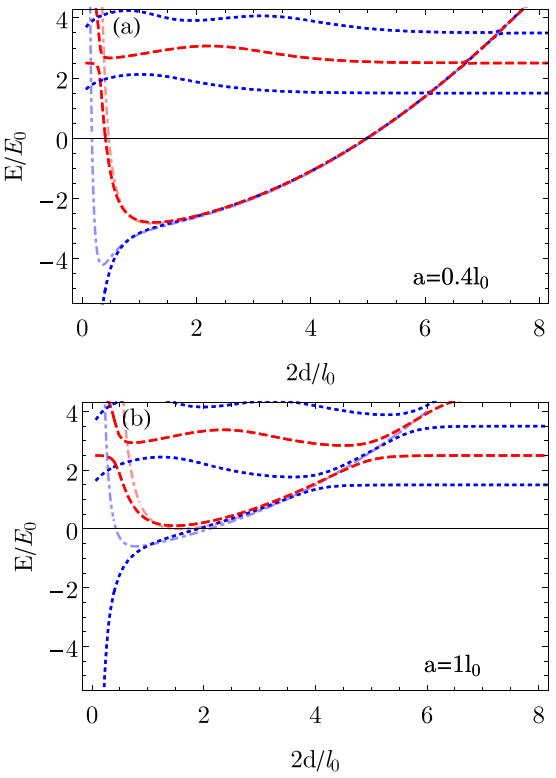

FIG. 4. The dependence of the lowest-energy levels on the distance $2d$ between the symmetrically placed impurities. The results are presented for $a = 0.4\,l_0$ [upper panel (a)] and $a = l_0$ [lower panel (b)]. The color code of the levels is the same as in Fig. 3. Additionally, the dotted-dashed lighter blue and lighter red lines represent the energies of the even and odd bound states, respectively, obtained within variational approach.

In Fig. 5 we show the zoom-in of the avoided crossing for $a/l_0 = 0.4$. The full, original results are depicted with dotted blue and dashed red curves, whereas lighter blue and lighter red colors are dedicated for the variational approach. Clearly, since the curves obtained within different methods collapse onto each other, the simple three-state model gives the quantitative description of the trap-induced resonance. Notice

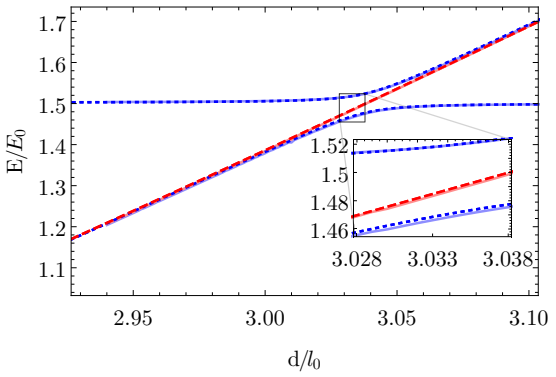

FIG. 5. Comparison of the results for $a = 0.4\,l_0$ in the vicinity of the lowest avoided crossing obtained within the full method (dotted blue and dashed red), and within the variational approach using three states (lighter blue and lighter red). The inset zooms the vicinity of the avoided crossing. The color code is the same as in Fig. 4.

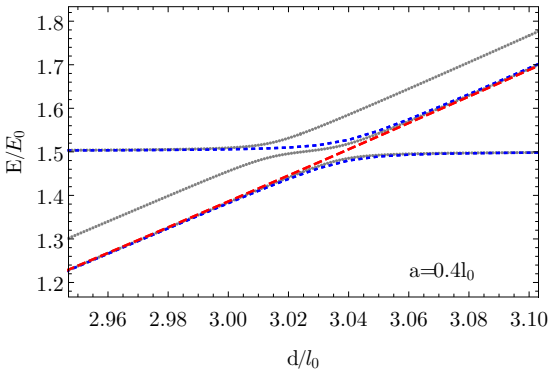

FIG. 6. Comparison of energy levels in the vicinity of avoided crossing. Red dashed line and blue dotted line denote odd and even states of the system with impurities placed symmetrically along the z axis in $z = \pm d$. Gray dotted line denotes the energy levels of the system, where the impurities are placed in $z = -d$ and $z = d + \Delta d$. Here, $\Delta d = 0.025 l_0$.

the presence of the state of different symmetry which passes through the avoided crossing (red dashed straight line) without being affected by the other states.

B. Asymmetric case

The states and the energy levels of the atom divide into separate classes, belonging to different irreducible representations of the symmetry group [37], characterized by different symmetry properties. Since $\mathbf{d}_1 = -\mathbf{d}_2$ the Hamiltonian is invariant with respect to the reflection in the plane passing in-between the impurities and perpendicular to the line joining the particles. To see how the coupling between the states affects the energy levels, we break the symmetry by perturbing one impurity's position. Now, the position $\mathbf{d}_2 = -d\mathbf{e}_z$ is unaffected, whereas $\mathbf{d}_1 = (d + \Delta d)\mathbf{e}_z$, where we denote by $\mathbf{e}_z$ the unit vector pointing along the z axis.

The energy levels of the atom in such a configuration with $\Delta d = 0.025 l_0$ are presented in Fig. 6. The dotted blue (even states) and dashed red (odd states) lines are the full solutions of the initial, unperturbed system, whereas the small-dotted gray line represents energy levels of the perturbed Hamiltonian. All the states are repelling, lifting the degeneracy, which results in two very close avoided crossings between these states and one of the extended state in the harmonic trap. This twin resonance, facilitated by the controlled symmetry breaking of the system and by the presence of the trap, signals the breakdown of the usual Landau-Zener theory [38–40].

C. Wave functions in the symmetric case of two impurities

With our method we also determine the wave function of the atom. Provided the coefficients k_i are known, the wave

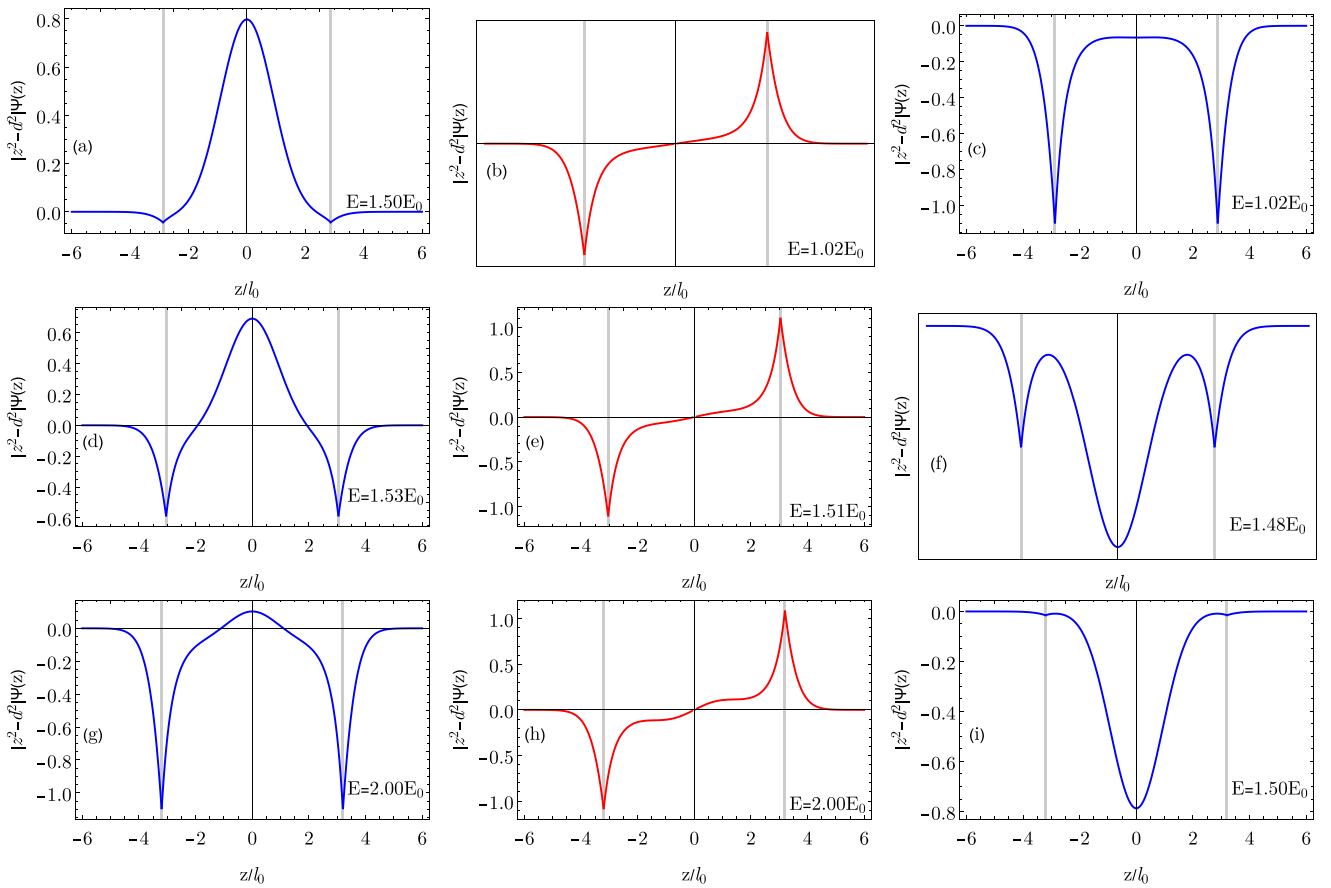

FIG. 7. Cuts along the z axis of the (renormalized) wave functions of the atom for different d and E with the scattering length $a = 0.4 l_0$ close to avoided crossings. Gray vertical lines denote the positions of the ions.

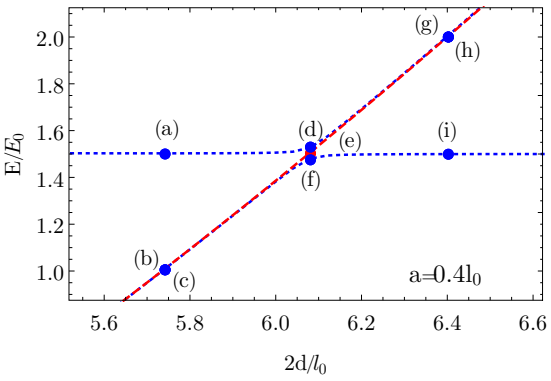

FIG. 8. The vicinity of the lowest avoided crossing for $a = 0.4l_0$. Red dashed line and blue dotted line denote odd and even states of the system with impurities placed symmetrically along the z axis in $z = \pm d$. The points marked with letters (a)–(i) indicate the parameter values for which the eigenstates are studied in Fig. 7.

function is evaluated from Eq. (4), and it takes the form

$$\Psi(\mathbf{r}) = \sum_{i=1}^{N} g_i k_i G(\mathbf{d}_i, \mathbf{r}). \tag{14}$$

In this sum, the energy E as well as the eigenstates are determined from Eq. (8). So far, we considered the energy levels of the atom, and therefore we already determined the matrix $\hat{D}_2(E)$, which in our case of two symmetrically placed impurities takes a dimensionless form of $\tilde{D}(E)$ [see Eq. (11)]. The solution is then particularly simple since the symmetry property imposes $k_1 = k_2$ for even states, and $k_1 = -k_2$ for odd states.

In Fig. 7, we present the cuts along the z axis of the wave functions of nine eigenstates in the vicinity of the lowest avoided crossing for $a = 0.4\,l_0$. For the clarity of presentation, we plot the wave functions multiplied by a factor $|z^2 - d^2|$ to remove the divergence, which appears for $z = \pm d$ and $x = y = 0$. Each divergence originates in the Green's function, which has a pole when its two arguments approach each other, i.e., $G(\mathbf{d}_i, \mathbf{r}) \propto 1/|\mathbf{r} - \mathbf{d}_i|$ for $\mathbf{r} \approx \mathbf{d}_i$. This divergence is responsible for the limiting behavior of the wave function at vanishing atom-impurity distance. According to the contact condition, $\Psi(\mathbf{r})$ is proportional to $1 - a/|\mathbf{r} - \mathbf{d}_i|$ in this case.

Figure 8 magnifies the relevant avoided crossing that we investigate here in more details. The nine points, marked with letters from (a) to (i), indicate the parameter values for which the eigenstates are presented on the plots in Figs. 7(a)–7(i). The points (a)–(c) correspond to the situation when the bound states of the atom-impurity interaction potential are lower in energy than the state of the trap (see Fig. 2). The point (a) indicates the trap extended, even state of the atom with small admixture of the states localized on the impurities. Figures 7(b) and 7(c) [corresponding to points (b) and (c) from Fig. 8] show the even and odd bound states of the atom. A similar situation occurs when the bound state of the atom-impurity interaction potential is slightly higher in energy than the trap state [plots (g)–(i) in Fig. 7 corresponding to points (g)–(i) in Fig. 8], where the wave functions are either localized mainly on the impurities [see the plots (g)–(h)] or delocalized in the trap [see the plot (i)].

In the region where trap-induced resonance is present [see Figs. 7(d)–7(f)], the trap extended state is mixed with the states localized on the impurities in the vicinity of the avoided crossing and corresponding amplitudes, v_1 and v_2, are of the same order. This is explained by the variational model embodied in Eq. (12). In addition to the states of the even symmetry, we find a localized wave function of the bound state with odd symmetry [see Fig. 7(e) corresponding to the red point (e) lying on the red dashed line in Fig. 8].

IV. SUMMARY

In this work, we presented a general method of solving the problem of a single atom interacting with N stationary impurities. The approach is based on the Green's function formalism, and assumes the contact potential approximation. The method can be applied for arbitrary arrangement of the impurities, even when the interaction strength is different for each one.

We applied the method to the case of two impurities placed in a spherical harmonic trap. We determined energies and wave functions of stationary states of the atom. The spectrum exhibits multiple avoided crossings between the bound states and the extended trap states. A simple three-states model correctly reproduces the bound states in the trap as well as the trap-induced resonances.

Our results can be further generalized to include energy-dependent scattering lengths, which would allow for more accurate treatment of long-range potentials, for instance, the atom-ion polarization potential [41]. The method, by providing single-particle orbitals, can serve as a starting point for more involved calculations, such as dynamics of the atom in complex quantum networks of impurities, or many-body system of weakly interacting bosons interacting with multiple trapped ions [42]. Assuming the Born-Oppenheimer approximation, which is valid for light atoms, it is possible to include motion of the impurities within the method, possibly capturing effects such as atom-phonon coupling [22].

This work presents a study of a simplified case in which the atom-impurity interaction is described using a zero-range potential. This is sufficient as long as the characteristic length scale of the interaction is much smaller than other length scales such as the interparticle distance. Within this treatment, the system has some characteristic features of a diatomic molecule such as the presence of even and odd states. However, the truly interesting case would be the one when the atom interacts strongly with many impurities at the same time, where the zero-range model does not apply. Experimental realization of such a system would require bringing the impurities within the characteristic atom-impurity interaction distance, e.g., hundreds of nanometers in the ion-atom case. This cannot currently be achieved with stationary impurities. Rigorous theoretical description of such a system would require including the motion of the impurities as well as using realistic interaction potentials, resulting in a numerically challenging problem. The current results can then serve as a limiting case.

ACKNOWLEDGMENTS

We thank A. Negretti and R. Gerritsma for valuable discussions. This work was supported by the National Science Centre, Poland Projects No. 2014/14/M/ST2/00015, No. DEC-2013/09/N/ST2/02188, and No. 2015/17/B/ST2/00592,

the Alexander von Humboldt Foundation, and German Research Foundation (DFG) Priority Program GiRyd.

APPENDIX A: SOLUTION OF THE SCHRÖDINGER EQUATION

In order to solve the Schrödinger equation for the atom [see Eq. (3)], we first expand the unknown wave function $\Psi(\mathbf{r}) = \sum_{\mathbf{n}} c_{\mathbf{n}}\phi_{\mathbf{n}}(\mathbf{r})$ in the basis $\phi_{\mathbf{n}}$ of the stationary states of the atom but without the impurities. Inserting the expansion of $\Psi(\mathbf{r})$ into Eq. (3), we obtain

$$\sum_{\mathbf{n}} c_{\mathbf{n}} E_{\mathbf{n}}\phi_{\mathbf{n}}(\mathbf{r}) + \sum_{i=1}^{N} g_i \delta(\mathbf{r}_i)\frac{\partial}{\partial r_i} r_i \left[\sum_{\mathbf{n}} c_{\mathbf{n}}\phi_{\mathbf{n}}(\mathbf{r})\right]_{\mathbf{r}\to\mathbf{d}_i} = E\sum_{\mathbf{n}} c_{\mathbf{n}}\phi_{\mathbf{n}}(\mathbf{r}), \tag{A1}$$

where $E_{\mathbf{n}}$ denotes the energy corresponding to the state $\phi_{\mathbf{n}}$. The next step is to project both sides of Eq. (A1) onto a single state of the basis $\phi^*_{\mathbf{m}}$, in order to determine the expansion coefficients $c_{\mathbf{m}}$:

$$\sum_{i=1}^{N} g_i \phi^*_{\mathbf{m}}(\mathbf{d}_i)\frac{\partial}{\partial r_i} r_i \left[\sum_{\mathbf{n}} c_{\mathbf{n}}\phi_{\mathbf{n}}(\mathbf{r})\right]_{\mathbf{r}\to\mathbf{d}_i} = (E - E_{\mathbf{m}})c_{\mathbf{m}}. \tag{A2}$$

Now, we replace back the expansion $\sum_{\mathbf{n}} c_{\mathbf{n}}\phi_{\mathbf{n}}(\mathbf{r})$ with $\Psi(\mathbf{r})$:

$$c_{\mathbf{m}}(E - E_{\mathbf{m}}) = \sum_{i=1}^{N} g_i \phi^*_{\mathbf{m}}(\mathbf{d}_i)\left[\frac{\partial}{\partial r_i} r_i \Psi(\mathbf{r})\right]_{\mathbf{r}\to\mathbf{d}_i}. \tag{A3}$$

Dividing both sides of Eq. (A3) by $(E - E_{\mathbf{m}})$, we finally obtain the equation for the expansion coefficients $c_{\mathbf{m}}$:

$$c_{\mathbf{m}} = \sum_{i=1}^{N} g_i k_i \frac{\phi^*_{\mathbf{m}}(\mathbf{d}_i)}{(E - E_{\mathbf{m}})}, \tag{A4}$$

where

$$k_i = \left[\frac{\partial}{\partial r_i} r_i \Psi(\mathbf{r})\right]_{\mathbf{r}\to\mathbf{d}_i}. \tag{A5}$$

Substituting Eq. (A4) into the expansion of $\Psi(\mathbf{r})$ yields the wave function in the following form:

$$\Psi(\mathbf{r}) = \sum_{i=1}^{N}\sum_{\mathbf{n}} g_i k_i \frac{\phi^*_{\mathbf{n}}(\mathbf{d}_i)\phi_{\mathbf{n}}(\mathbf{r})}{(E - E_{\mathbf{n}})} = \sum_i k_i G(\mathbf{d}_i,\mathbf{r}), \tag{A6}$$

where $G(\mathbf{d}_i,\mathbf{r}) = \sum_{\mathbf{n}} \phi^*_{\mathbf{n}}(\mathbf{d}_i)\phi_{\mathbf{n}}(\mathbf{r})/(E - E_{\mathbf{n}})$ is the Green's function (see Appendix B for details), and, therefore, we arrive at the consistency condition given by

$$k_i = \sum_{j=1}^{N} g_j k_j \left[\frac{\partial}{\partial r_i} r_i G(\mathbf{d}_j,\mathbf{r})\right]_{\mathbf{r}\to\mathbf{d}_i}. \tag{A7}$$

Here, we notice that in the case of $i \neq j$ the regularization operator is redundant, i.e., $[\frac{\partial}{\partial r_i} r_i G(\mathbf{d}_j,\mathbf{r})]_{\mathbf{r}\to\mathbf{d}_i} = G(\mathbf{d}_i,\mathbf{d}_j)$. Therefore, the condition in Eq. (A7) can be rewritten in the form of $\hat{D}_N(E)\cdot\vec{k} = 0$, with $\hat{D}_N(E)$ given by Eq. (9).

APPENDIX B: GREEN'S FUNCTION FOR SPHERICALLY SYMMETRIC HARMONIC POTENTIAL

We discuss here the properties of the Green's function for an isotropic three-dimensional (3D) harmonic oscillator. The analytical formulas for n dimensions were found in [43]. In the case of an anisotropic harmonic trap, the Green's function can be expressed in terms of an integral that has to be calculated numerically [44]. The Green's function of a system described by the Hamiltonian H_0 is defined by

$$(H_0 - E)G(\mathbf{r},\mathbf{r}') = -\delta(\mathbf{r} - \mathbf{r}'). \tag{B1}$$

This equation can be solved by expanding G in the basis of H_0, i.e., 3D harmonic oscillator wave functions in our case, and the final expression is

$$G(\mathbf{r}',\mathbf{r}) = \sum_{\mathbf{n}} \frac{\phi^*_{\mathbf{n}}(\mathbf{r}')\phi_{\mathbf{n}}(\mathbf{r})}{E - E_{\mathbf{n}}}, \tag{B2}$$

where $\phi_{\mathbf{n}}$ is the eigenfunction of H_0 with eigenvalue $E_{\mathbf{n}}$. This expression is exactly the one in Eq. (6).

The Green's function of the isotropic harmonic oscillator was calculated analytically in [45], and is given in terms of the confluent hypergeometric functions U and M:

$$G(\mathbf{r},\mathbf{r}') = \exp\left(-\frac{\xi+\eta}{2}\right)\left\{\Lambda(1,E)\left[1 + \frac{2\xi\eta}{\xi-\eta}\left(\frac{\partial}{\partial\eta} - \frac{\partial}{\partial\xi}\right)\right]U^{(1)}_E(\xi)M^{(1)}_E(\eta) + \mathrm{sign}(\mathbf{r}\cdot\mathbf{r}')\Lambda(1,E+1)\frac{2\sqrt{\xi\eta}}{\xi-\eta}\left(\eta\frac{\partial}{\partial\eta} - \xi\frac{\partial}{\partial\xi}\right)U^{(1)}_{E+1}(\xi)M^{(1)}_{E+1}(\eta)\right\}, \tag{B3}$$

where the function Λ is expressed in terms of the Euler gamma function

$$\Lambda(1,E) = -\frac{1}{2}\left(\frac{1}{\pi}\right)^{3/2}\Gamma\left(\frac{3}{4} - \frac{E}{2}\right), \tag{B4}$$

while the dimensionless parameters ξ and η depend on the positions $\mathbf{r}$ and $\mathbf{r}'$:

$$\xi = \tfrac{1}{2}(r^2 + r'^2 + |\mathbf{r} - \mathbf{r}'||\mathbf{r} + \mathbf{r}'|), \tag{B5}$$

$$\eta = \tfrac{1}{2}(r^2 + r'^2 - |\mathbf{r} - \mathbf{r}'||\mathbf{r} + \mathbf{r}'|). \tag{B6}$$

The derivatives of the confluent hypergeometric functions U and M are, respectively, given by [45]

$$\frac{\partial}{\partial\xi}U(a,b,\xi) = -aU(a+1,b+1,\xi), \tag{B7}$$

$$\frac{\partial}{\partial\eta}M(a,b,\eta) = \frac{a}{b}M(a+1,b+1,\eta). \tag{B8}$$

To proceed, let us further introduce the following notation for the sake of brevity:

$$F^{(n)}_E(x) \equiv F\left(\frac{4n-1}{4} - \frac{E}{2}, \frac{2n+1}{2}, x\right),$$

where F denotes the confluent hypergeometric function U or M, parameter n is an integer, and x denotes ξ or η defined in Eqs. (B5) and (B6), respectively.

Substituting the derivatives into Eq. (B3), we obtain the following expression for the Green's function:

$$G(\mathbf{r},\mathbf{r}') = \exp\left(-\frac{\xi+\eta}{2}\right)\left\{\Lambda(1,E)U_E^{(1)}(\xi)M_E^{(1)}(\eta) + \frac{2\xi\eta}{\xi-\eta}\Lambda(1,E)\left(\frac{3}{4}-\frac{E}{2}\right)\left[\frac{2}{3}U_E^{(1)}(\xi)M_E^{(2)}(\eta) + U_E^{(2)}(\xi)M_E^{(1)}(\eta)\right]\right.$$
$$\left. + \mathrm{sign}(\mathbf{r}\cdot\mathbf{r}')\Lambda(1,E+1)\frac{2\sqrt{\xi\eta}}{\xi-\eta}\left(\frac{3}{4}-\frac{E}{2}\right)\left[\frac{2}{3}\eta U_{E+1}^{(1)}(\xi)M_{E+1}^{(2)}(\eta) + \xi U_{E+1}^{(2)}(\xi)M_{E+1}^{(1)}(\eta)\right]\right\}. \quad \text{(B9)}$$

Expanding Eq. (B9) in the Taylor series, we obtain the following asymptotic behavior for in the limit when $\mathbf{r}'$ approaches $\mathbf{r}$:

$$G(\mathbf{r},\mathbf{r}') \xrightarrow{\Delta r\to 0} g^0(R) + \frac{g^1(R)}{\Delta r}, \quad \text{(B10)}$$

where the distance between the points $\mathbf{r}$ and $\mathbf{r}'$ is denoted by $\Delta r = |\mathbf{r}-\mathbf{r}'|$, the mean position is given by $R = |\mathbf{r}+\mathbf{r}'|/2$, and the functions g^0 and g^1 are, respectively, given by

$$\begin{aligned} g^0(R) = {} & -\tfrac{1}{4}\Lambda(1,E)\exp(-R^2)\big\{4RM_E^{(1)}(R^2)U_E^{(1)}(R^2) - \tfrac{1}{3}(2E-3)R^5\big[2(2E-7)M_E^{(3)}(R^2)U_E^{(3)}(R^2) \\ & + 10(2E-3)M_E^{(2)}(R^2)U_E^{(2)}(R^2)\big] + 15(2E-7)M_E^{(1)}(R^2)U_E^{(3)}(R^2)\big\} \\ & - \tfrac{1}{60}\mathrm{sign}(\mathbf{r}\cdot\mathbf{r}')(2E-1)\Lambda(1,E+1)\exp(-R^2)R^2\big\{(-5+2E)R^2M_{E+1}^{(3)}(R^2)U_{E+1}^{(1)}(R^2) \\ & - 10M_{E+1}^{(2)}(R^2)\big[U_{E+1}^{(1)}(R^2) + (2-4E)R^2U_{E+1}^{(2)}(R^2)\big] + 15M_{E+1}^{(1)}(R^2)\big[U_{E+1}^{(2)}(R^2) + (2E-5)R^2U_{E+1}^{(3)}(R^2)\big]\big\}, \quad \text{(B11a)} \\ g^1(R) = {} & -\tfrac{1}{12}\Lambda(1,E)(2E-3)\exp(-R^2)\big[2M_E^{(2)}(R^2)U_E^{(1)}(R^2) + 3M_E^{(1)}(R^2)U_E^{(2)}(R^2)\big] \\ & -\mathrm{sign}(\mathbf{r}\cdot\mathbf{r}')\tfrac{1}{12}\Lambda(1,E+1)(2E-1)e^{-R^2}R^3\big[2M_{E+1}^{(2)}(R^2)U_{E+1}^{(1)}(R^2) + 3M_{E+1}^{(1)}(R^2)U_{E+1}^{(2)}(R^2)\big]. \quad \text{(B11b)} \end{aligned}$$

[1] I. Bloch, J. Dalibard, and W. Zwerger, Rev. Mod. Phys. **80**, 885 (2008).
[2] M. Lewenstein, A. Sanpera, V. Ahufinger, B. Damski, A. Sen, and U. Sen, Adv. Phys. **56**, 243 (2007).
[3] C. Chin, R. Grimm, P. Julienne, and E. Tiesinga, Rev. Mod. Phys. **82**, 1225 (2010).
[4] M. Greiner, O. Mandel, T. Esslinger, T. W. Hänsch, and I. Bloch, Nature (London) **415**, 39 (2002).
[5] S. Trotzky, P. Cheinet, S. Fölling, M. Feld, U. Schnorrberger, A. M. Rey, A. Polkovnikov, E. Demler, M. Lukin, and I. Bloch, Science **319**, 295 (2008).
[6] M. Schreiber, S. S. Hodgman, P. Bordia, H. P. Lüschen, M. H. Fischer, R. Vosk, E. Altman, U. Schneider, and I. Bloch, Science **349**, 842 (2015).
[7] J. Léonard, A. Morales, P. Zupancic, T. Esslinger, and T. Donner, Nature (London) **543**, 87 (2017).
[8] J.-R. Li, J. Lee, W. Huang, S. Burchesky, B. Shteynas, F. Ç. Top, A. Jamison, and W. Ketterle, Nature (London) **543**, 91 (2017).
[9] D. Jaksch, J. I. Cirac, P. Zoller, S. L. Rolston, R. Côté, and M. D. Lukin, Phys. Rev. Lett. **85**, 2208 (2000).
[10] R. Stock, I. H. Deutsch, and E. L. Bolda, Phys. Rev. Lett. **91**, 183201 (2003).
[11] E. Charron, M. A. Cirone, A. Negretti, J. Schmiedmayer, and T. Calarco, Phys. Rev. A **74**, 012308 (2006).
[12] D. Hayes, P. S. Julienne, and I. H. Deutsch, Phys. Rev. Lett. **98**, 070501 (2007).
[13] H. Doerk, Z. Idziaszek, and T. Calarco, Phys. Rev. A **81**, 012708 (2010).
[14] A. Negretti, P. Treutlein, and T. Calarco, Quantum Inf. Proc. **10**, 721 (2011).
[15] K. Jachymski, Z. Idziaszek, and T. Calarco, Phys. Rev. Lett. **112**, 250502 (2014).
[16] D. Leibfried, R. Blatt, C. Monroe, and D. Wineland, Rev. Mod. Phys. **75**, 281 (2003).
[17] M. Saffman, T. G. Walker, and K. Mølmer, Rev. Mod. Phys. **82**, 2313 (2010).
[18] D. J. Wineland, Rev. Mod. Phys. **85**, 1103 (2013).
[19] S. Haroche, Rev. Mod. Phys. **85**, 1083 (2013).
[20] M. Tomza, K. Jachymski, R. Gerritsma, A. Negretti, T. Calarco, Z. Idziaszek, and P. S. Julienne, arXiv:1708.07832.
[21] J. M. Schurer, A. Negretti, and P. Schmelcher, Phys. Rev. Lett. **119**, 063001 (2017).
[22] U. Bissbort, D. Cocks, A. Negretti, Z. Idziaszek, T. Calarco, F. Schmidt-Kaler, W. Hofstetter, and R. Gerritsma, Phys. Rev. Lett. **111**, 080501 (2013).
[23] D. Barredo, S. de Léséleuc, V. Lienhard, T. Lahaye, and A. Browaeys, Science **354**, 1021 (2016).
[24] M. Endres, H. Bernien, A. Keesling, H. Levine, E. R. Anschuetz, A. Krajenbrink, C. Senko, V. Vuletic, M. Greiner, and M. D. Lukin, Science **354**, 1024 (2016).
[25] H. Bernien, S. Schwartz, A. Keesling, H. Levine, A. Omran, H. Pichler, S. Choi, A. S. Zibrov, M. Endres, M. Greiner *et al.*, Nature (London) **551**, 579 (2017).
[26] D. Barredo, V. Lienhard, S. de Léséleuc, T. Lahaye, and A. Browaeys, arXiv:1712.02727.
[27] K. Huang and C. N. Yang, Phys. Rev. **105**, 767 (1957).
[28] M. Antezza, Y. Castin, and D. A. W. Hutchinson, Phys. Rev. A **82**, 043602 (2010).
[29] D. Blume and C. H. Greene, Phys. Rev. A **65**, 043613 (2002).

[30] E. L. Bolda, E. Tiesinga, and P. S. Julienne, Phys. Rev. A **66**, 013403 (2002).
[31] M. Wouters and G. Orso, Phys. Rev. A **73**, 012707 (2006).
[32] Z. Idziaszek, Phys. Rev. A **79**, 062701 (2009).
[33] T. Busch, B. Englert, K. Rzążewski, and M. Wilkens, Found. Phys. **28**, 549 (1998).
[34] G. L. Guo, K. T. Tang, J. P. Toennies, and C. L. Yiu, J. Chem. Phys. **98**, 8777 (1993).
[35] M. Krych and Z. Idziaszek, Phys. Rev. A **80**, 022710 (2009).
[36] Z. Idziaszek, T. Calarco, and P. Zoller, Phys. Rev. A **76**, 033409 (2007).
[37] L. D. Landau and E. Lifshitz, *Course of Theoretical Physics, Vol. 3, Quantum Mechanics* (Pergamon Press, Oxford, 1958).
[38] C. E. Carroll and F. T. Hioe, J. Phys. A: Math. Gen. **19**, 1151 (1986).
[39] C. E. Carroll and F. T. Hioe, J. Opt. Soc. Am. B **2**, 1355 (1985).
[40] A. V. Shytov, Phys. Rev. A **70**, 052708 (2004).
[41] V. S. Melezhik and A. Negretti, Phys. Rev. A **94**, 022704 (2016).
[42] J. M. Schurer, R. Gerritsma, P. Schmelcher, and A. Negretti, Phys. Rev. A **93**, 063602 (2016).
[43] V. L. Bakhrakh, S. I. Vetchinkin, and S. V. Khristenko, Theor. Math. Phys. **12**, 776 (1972).
[44] Z. Idziaszek and T. Calarco, Phys. Rev. A **71**, 050701 (2005).
[45] D. Khrebtukov and J. Macek, J. Phys. A: Math. Gen. **31**, 2853 (1998).